Chapter 11

Fatigue Crack Propagation Rates Prediction Using Probabilistic Strain-Based Models

José António Fonseca De Oliveira Correia,
Abílio M.P. De Jesus, Pedro M.G.P. Moreira,
Rui A.B. Calçada and Alfonso Fernández-Canteli

Additional information is available at the end of the chapter

http://dx.doi.org/10.5772/64829

Abstract

This chapter proposes an evaluation and extension of the UniGrow model to predict the fatigue crack propagation rate, based on a local strain-based approach to fatigue. The UniGrow model, classified as a residual stress-based crack propagation model, is here applied to derive probabilistic fatigue crack propagation fields (p-da/dN-ΔK-R fields) for P355NL1 pressure vessel steel, covering distinct stress R-ratios. The results are compared with available experimental data. The required strain-life data are experimentally achieved and evaluated. The material representative element size, ϱ^*, a key parameter in the UniGrow model, is assessed by means of a trial-and-error procedure of inverse analysis. Moreover, residual stresses are computed for varying crack lengths and minimum-to-maximum stress ratios. Elastoplastic stress fields around the crack apex are evaluated with analytical relations and compared with elastoplastic finite-element (FE) computations. The deterministic strain-life relations proposed in the original UniGrow model are replaced by the probabilistic strain-life fields (p-ε-N) proposed by Castillo and Canteli. This probabilistic model is also extended by considering a damage parameter to allow for mean stress effects. In particular, a probabilistic Smith-Watson-Topper field (p-SWT-N), alternatively to the conventional p-ε-N field, is proposed and applied to derive the probabilistic fatigue crack propagation fields.

Keywords: fatigue crack propagation, fracture mechanics, local fatigue approaches, probabilistic models, P355NL1 steel

1. Introduction

Research about the fatigue behaviour of materials and structures has engaged both academia and industry. Fatigue has been investigated since the industrial revolution and remains an unsolved research topic due to the lack of reliable predictive models and the continuous emergent materials and applications [1]. The knowledge on fatigue crack propagation is not fully accomplished, despite the great advances achieved in the last decades. In particular, probabilistic approaches are still lacking.

Paris et al. [2] were the first to establish a correlation between the fatigue crack propagation rates and the stress intensity factor, suggesting the well-known and widely accepted Paris' law. Since this contribution, the pioneer Paris' law has been used extensively to model fatigue crack growth under constant amplitude loading but also under random loading. However, Paris' law shows some limitations, as it only models the stable crack propagation regime, excluding near threshold and near unstable fatigue crack propagation phases, and the stress ratio effects are not accounted for. Further, it is a deterministic approach for fatigue crack propagation. Many other fatigue crack propagation relations have been suggested in the literature to solve the shortcomings of the Paris' law including enhanced prediction of fatigue crack growth under variable amplitude loading [3]. The assortment of fatigue crack propagation models available in the literature differs in the number of variables and parameters involved and the application domains. However, their use requires the evaluation of expensive time-consuming fatigue crack propagation tests in order to identify their constants.

Local fatigue strain-based approaches [4–7] represent an alternative to the fracture mechanics fatigue crack propagation once the former being very often applied to model the fatigue crack initiation on notched components [8]. They are usually complemented with fracture mechanics models to allow full fatigue life assessments.

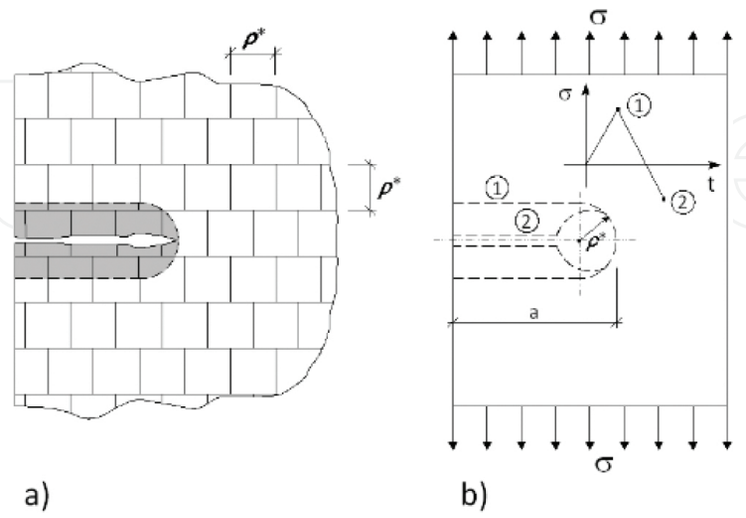

Figure 1. Crack discretization according to the UniGrow model: (a) crack and discrete elementary material blocks and (b) crack shape at the tensile maximum and compressive minimum loads [11].

http://dx.doi.org/10.5772/64829

Some authors, as Glinka [9], Peeker and Niemi [10], Noroozi et al. [11–13] and Hurley and Evans [14], have applied local strain-based fatigue models to represent fatigue crack propagation. Glinka was one of the precursors of modelling fatigue crack propagation using a strain-based fatigue relation [9]. The crack was assumed to have a notch with a tip radius, ρ^*, and the material ahead of the crack tip was assumed to be divided into elemental blocks of finite linear dimension, ρ^* (see **Figure 1**). The crack growth was assumed as the failure of the successive elemental blocks, the fatigue crack growth rate being defined by the following relation:

$$\frac{da}{dN} = \frac{\rho^*}{N_f} \tag{1}$$

where N_f represents the number of cycles to fail the elemental block of dimension, ρ^*. This approach allowed the fatigue crack growth rate to be directly expressed by the strain-life relation constants.

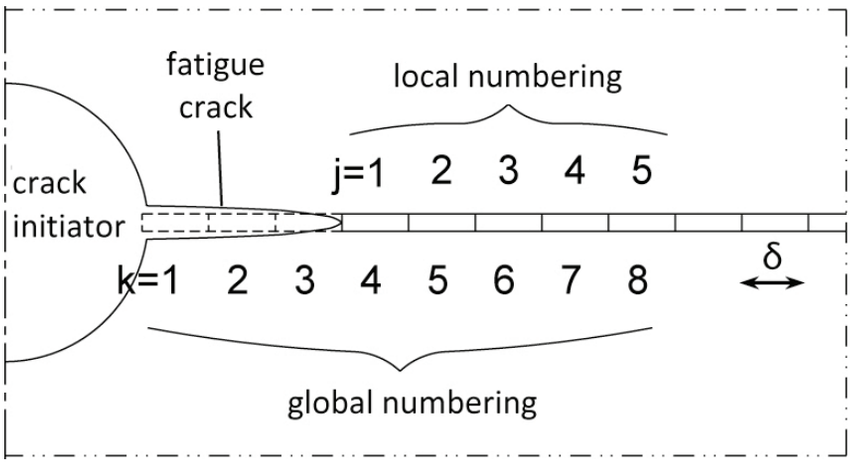

Figure 2. Crack discretization with elements according to the model proposed by Peeker and Niemi [10].

Similarly, the model proposed by Peeker and Niemi [10] allowed the near threshold fatigue crack propagation data and the stable crack growth to be described (see **Figure 2**). For the near threshold fatigue crack propagation, the authors derived the following analytical relation functions of the strain-life constants:

$$\begin{aligned} &\frac{da}{dN} = C_{el}\Delta K^{m_{el}} \\ &C_{el} = 2\delta\left[\left(\sigma_f' - \sigma_m\right)\sqrt{2\pi\delta}\right]^{\frac{1}{b'}} \\ &m_{el} = -\frac{1}{b'} \end{aligned} \tag{2}$$

For the stable crack growth, the above authors derived the following alternative relations that use the cyclic stress-strain constants besides the elastoplastic strain-life constants:

$$\frac{da}{dN} = C_{pl}\Delta K^{m_{pl}}$$

$$C_{pl} = 2\delta\left[\varepsilon'_f\left(\frac{4\pi\delta K'E}{n'+1}\right)^{\frac{1}{n'+1}}\right]^{\frac{1}{c'}} \tag{3}$$

$$m_{pl} = -\frac{2}{c'(n'+1)}$$

The superposition of the two previous relations leads to the following analytical expression for the fatigue crack propagation law covering both fatigue propagation regimes I and II:

$$\frac{da}{dN} = \frac{1}{\frac{1}{C_{pl}\Delta K^{m_{pl}}} + \frac{1}{C_{el}\Delta K^{m_{el}}}} \tag{4}$$

The application of the local approaches to fatigue on fatigue crack growth simulation requires the definition of a crack path discretization. The size of the elements used to discretize the crack path should account for two criteria: (a) the size must be large enough to represent the local material properties by their mean values using continuous variables and (b) its size should be related to micro-structural material parameters, such as the material grain size. For structural steels, and according to reference [10], the criteria result in an average element size of 0.1 mm = 100 μm.

In general, elastoplastic stress analysis at the crack vicinity is required and very often analytical approaches are applied. Nonetheless, Hurley and Evans [14] proposed the use of elastoplastic finite-element analysis. The fatigue life of the process zone was computed using the Walker strain that was correlated directly with the fatigue life from the experimental data using a power relation. This Walker strain is defined according to the following relation:

$$\varepsilon_w = \frac{\sigma_{max}}{E}\left(\frac{\Delta\varepsilon E}{\sigma_{max}}\right)^w \tag{5}$$

where σ_{max} is the maximum stress, E is the Young modulus, $\Delta\varepsilon$ is the strain range and w is a constant varying between 0 and 1. These authors applied the following definition of the cyclic plastic zone that is assumed equal to the fatigue process damage zone under plane strain conditions:

$$\Delta a_i = \frac{1}{3\pi}\left(\frac{\Delta K}{2\sigma_0}\right)^2 \tag{6}$$

where σ_0 is the cyclic yield stress and ΔK is the stress intensity factor range computed from the numerical model. The resulting approach is much simpler than those proposed by previous authors. It is supported by numerical models disregarding analytical aspects that allowed

http://dx.doi.org/10.5772/64829

previous authors to verify the relation between these local approaches to fatigue and the fracture mechanics approaches for fatigue crack propagation.

In all previous studies, the fatigue crack growth process has been modelled as a continuous damaging process consisting of successive failure of material elements along the assumed crack path. These crack propagation approaches have provided accurate correlations of crack propagation data from several sources that included the stress ratio or mean stress effects. These crack propagation approaches are local fatigue approaches, where the stress-strain fields ahead of the crack tip are computed supported by elastoplastic stress-strain analyses. The resulting elastoplastic stress-strain fields are used in fatigue damage analysis performed for each material element in the crack path. Analytical methods such as the ones proposed by Neuber [15] and Moftakhar et al. [16] may be applied to perform the elastoplastic analysis taking into account the elastic stress-strain fields computed around the crack tip, using available linear elastic fracture mechanics solutions [11, 16, 17].

This chapter proposes an evaluation and extension of the model proposed by Noroozi et al. [11–13] to predict the fatigue crack propagation rates, based on a local strain-life fatigue approach. This model denoted that the UniGrow model is a residual stress-based crack propagation model [18]. The model is adapted in this work to derive probabilistic fatigue crack propagation fields (p-da/dN-ΔK-R fields) for P355NL1 pressure vessel steel, covering distinct stress R-ratios. The procedure proposed has been already applied to other available experimental data [19–21]. The required strain-life data is experimentally evaluated and can be found in the literature [21]. The material representative element size, ρ^*, a key parameter in the UniGrow model, is assessed by means of a trial and error process. The residual stress field at crack tip vicinity is investigated for various crack lengths and minimum-to-maximum stress ratios. The elastoplastic stress-strain fields evaluated at the vicinity of the crack tip, using analytical solutions, are compared with the stress-strain fields computed using nonlinear elastoplastic finite-element analyses of the tested compact tension (CT) specimens considered in a fatigue crack propagation experimental program.

Deterministic strain-life relations proposed in the UniGrow model are replaced by the probabilistic strain-life fields (p-ε_a-N) proposed by Castillo and Canteli [22]. This probabilistic model is also extended by considering a damage parameter able to account for mean stress effects. In particular, a probabilistic Smith-Watson-Topper field (p-SWT-N) is proposed alternatively to the p-ε_a-N and applied to derive the probabilistic crack propagation fields.

2. Overview of the deterministic UniGrow model

The UniGrow model, originally developed by Noroozi et al. [11], rest on the following premises:

- A continuous material is discretized into elementary finite particles (dimension ρ^*), below which material continuity is no longer assured, (**Figure 1a**).

- The fatigue crack tip geometry exhibits a finite radius equivalent to a round notch of radius ρ^*, (**Figure 1b**).
- The fatigue crack growth is decomposed into successive crack increments, each one of equal size—the material elementary finite particle size. Therefore, this damaging process can be assumed as a continuous crack initiation process occurring at the material element levels characterized by the size ρ^*.
- The fatigue crack growth rate can then be computed using Eq. (1) and the number of cycles required to completely crack the material elementary particles can be computed by a local fatigue relation such as the ones based on a strain-life approach.

Noroozi et al. [11] proposed the application of the Smith, Watson and Topper fatigue damage parameter (SWT damage parameter) [7] in the form of the following fatigue life relation:

$$\sigma_{max} \cdot \Delta\varepsilon/2 = SWT = \left(\sigma_f'\right)^2 \cdot \left(2N_f\right)^{2b}/E + \sigma_f' \cdot \varepsilon_f' \cdot \left(2N_f\right)^{b+c} \tag{7}$$

Peeker and Niemi [10] propose, alternatively, the use of the Morrow's equation [6] to compute the failure of the material's representative element:

$$\frac{\Delta\varepsilon}{2} = \frac{\sigma_f' - \sigma_m}{E} \cdot \left(2N_f\right)^b + \varepsilon_f' \cdot \left(2N_f\right)^c \tag{8}$$

The Morrow's equation is derived from the following Coffin-Manson relation [4, 5] of the material, in order to include mean stress effects:

$$\frac{\Delta\varepsilon}{2} = \frac{\sigma_f'}{E} \cdot \left(2N_f\right)^b + \varepsilon_f' \cdot \left(2N_f\right)^c \tag{9}$$

In particular, Eq. (7) is derived by the multiplication of the Coffin-Manson Eq. (9) by the Basquin relation [23], for a fully reversal stress ratio, i.e. R ($\sigma_{min}/\sigma_{max}$) = –1, given by

$$\frac{\Delta\sigma}{2} = \sigma_{max} = \sigma_f' \cdot \left(2N_f\right)^b \tag{10}$$

In the previous two equations, σ_f' and b represent, respectively, the fatigue strength coefficient and exponent; ε_f' and c represent, respectively, the fatigue ductility coefficient and exponent and E is the Young modulus. The maximum stress, σ_{max}, mean stress, σ_m, and the strain range, $\Delta\varepsilon$, are computed and averaged over the material elementary size ρ^* using an elastoplastic analysis. According to Noroozi et al. [11, 12], the elastoplastic analysis can be performed, following the steps below, in order to estimate the stresses and strains at the elementary material elements placed along the crack path:

http://dx.doi.org/10.5772/64829

i. Application of the Creager-Paris solution [24] to evaluate the elastic stresses in the material region surrounding the crack tip.

ii. Application of analytical elastoplastic formulae such as the Neuber's [15] or Glinka's approaches [25] to transform the elastic stress field into actual elastoplastic stresses and strains ahead of the crack tip. Procedures by Moftakhar et al. [16] and Reinhard et al. [17] may also be applied to perform multi-axial elastoplastic stress-strain analysis.

iii. Determination of the residual stresses along the y-axis direction (normal to crack face) and along the crack path direction (line ahead of the crack tip), using the actual elastoplastic stresses computed at the end of the first load reversal and subsequent cyclic elastoplastic stress range, that is

$$\sigma_r = \sigma_{max} - \Delta\sigma \tag{11}$$

iv. Assuming the residual stress distribution computed ahead of the crack tip to be applied on the crack faces, behind the crack tip, in a symmetric way with respect to the crack tip ($x = 0$), the loading process generates a plastic zone at the crack tip that does not vanish completely during unloading, leading to a cyclic plastic zone, which is controlled by compressive stresses ahead of the crack tip and to some amount of crack opening displacement just behind the crack tip (crack faces does not close completely just behind the crack tip). One way to model crack opening consists in assuming that the compressive residual stress field acting ahead of the crack tip is applied in a symmetrical way, behind the crack tip, directly on crack faces. This compressive stress distribution acting on crack faces is equivalent to a residual stress intensity factor being used to correct the applied stress intensity factor range leading to a total (effective) stress intensity factor range that excludes the effects of the compressive stresses. It is proposed by Noroozi et al. [11, 12] to calculate the residual stress intensity factor, K_r, using the weight function method [26]:

$$K_r = \int_0^a \sigma_r(x) \cdot m(x,a)dx \tag{12}$$

where $m(x,a)$ is the weight function and σ_r is the residual stress field.

v. The applied stress intensity factor values (maximum and range) are corrected using the calculated residual stress intensity, resulting the total $K_{max,tot}$ and ΔK_{tot} values [11, 12]. For positive stress R-ratios, which corresponds to the range covered by the experimental data used in this research, $K_{max,tot}$ and ΔK_{tot} may be computed as follows:

$$\begin{aligned} K_{max,tot} &= K_{max,applied} + K_r \\ \Delta K_{tot} &= \Delta K_{applied} + K_r \end{aligned} \tag{13}$$

where K_r assumes a negative value corresponding to the compressive stress field. For high stress R-ratios, the compressive stresses ahead of the crack tip may be neglected and the applied stress intensity factor range is assumed fully effective and for low stress R-ratios, the compressive stresses increase and the effectiveness of the applied stress intensity factor range decreases.

vi. Using the total values of the stress intensity factors, the first and second steps (steps (i) and (ii)) are repeated to determine the corrected values for the maximum actual stress and actual strain ranges at the material's representative elements. Then, Eq. (7) is applied together with Eq. (1) to compute the fatigue crack growth rates in the original UniGrow model proposition.

The above fatigue crack propagation methodology does not provide close-form expressions for the fatigue crack propagation rates. Nevertheless, considering the material to behave according to dominant elastic or plastic behaviours at the crack tip, close-form solutions for the fatigue crack propagation rates are viable, leading to fatigue crack propagation relations based on two crack-driven parameters with the following form [11, 12]:

$$\frac{da}{dN} = C\left[\left(K_{max,tot}\right)^{p}\left(\Delta K_{tot}\right)^{q}\right]^{\gamma} \tag{14}$$

where C, p, q and γ are constants that can be related with the ones characterizing the cyclic elastoplastic behaviour of the material at the crack tip and the plasticity or elasticity dominance. The dependency of the fatigue crack propagation rates with both the maximum and range of stress intensity factors, $K_{\max}$ and ΔK, allows the mean stress effects to be conveniently accounted on fatigue crack propagation rates. This type of fatigue crack propagation model based on the combination of two parameters crack driving force has recently being proposed by several authors [27, 28].

In this chapter, the methodology proposed by Noroozi et al. [11] is followed with some variations. Material cyclic/fatigue properties are required. In addition, the UniGrow model introduces the material element size, ρ^*, which consists in an additional model parameter that in most of the situations needs to be computed by means of a trial and error iterative approach, in order to result in a good fitting of available experimental fatigue crack propagation data. The analytical elastoplastic analysis, supported by the Creager-Paris [24] elastic solutions and the Neuber's multi-axial approach [15–17], is applied to evaluate the elastoplastic stress-strain field at the first material element at the crack tip. Concerning the residual stresses along the crack path line, it is computed using a nonlinear elastoplastic finite-element analysis overcoming discrepancies verified in the analytical residual stress distributions, as demonstrated later in the chapter.

http://dx.doi.org/10.5772/64829

3. Modelling cyclic plasticity

In the following an elastoplastic constitutive model based on the von Mises yield criterion (J2 plasticity) and associative flow rule is selected to model compact tension specimen's elasto-plastic behaviour and particularly to compute the residual stresses at the fatigue crack region. Multi-linear kinematic hardening is used, which is crucial for the cyclic plasticity simulation and in particular the Bauschinger effect description. The von Mises yield criterion points out a yield function, *f*, defined as follows:

$$f = \left[\frac{3}{2}(S_{ij} - X_{ij})(S_{ij} - X_{ij})\right]^{1/2} - \sigma_k \leq 0 \tag{15}$$

where S_{ij} is the deviatoric stress tensor defined as

$$S_{ij} = \sigma_{ij} - \sigma_h \delta_{ij} \tag{16}$$

X_{ij} is the back-stress tensor that defines the translation of the yield surface, σ_k is the yield stress of the material, σ_{ij} is the stress state of the material, σ_h is the pressure or hydrostatic stress state and δ_{ij} is the Kronecker delta operator. The plastic flow occurs according to the associative flow rule, which means that the plastic strain increment can be computed from the derivatives of the yield function with respect to the stress tensor:

$$\dot{\varepsilon}_{ij}^{P} = \lambda \frac{\partial f}{\partial \sigma_{ij}} \tag{17}$$

where λ is the plastic multiplier related to the amount of plastic deformation. The adopted kinematic hardening rule is based on the Besseling model that is a sub-layer or overlay model [29] with the material behaviour, being composed of various portions (or sub-volumes), all subjected to the same total strain but each sub-volume having a different yield stress. Despite each sub-volume shows a simple stress-strain response, when combined, the model can represent multi-linear stress-strain curves. The following phases are performed in the plasticity calculations [30]:

i. The portion of total volume (the weighting factor) for each sub-volume and its corresponding yield stress are computed.

ii. For each sub-volume, the respective increment of the plastic strain is determined, assuming that each one is subjected to the same total strain.

iii. The individual increments in the plastic strain are summed up using the weighting factors determined in step (i) to result the total or apparent increment in plastic strain.

iv. The plastic strain is updated and the elastic strain is evaluated.

The weighting factor and yield stress for each sub-volume are determined by fitting the material response to the uniaxial stress-strain curve. A perfectly plastic material based on von Mises criterion is assumed. The weighting factor for sub-volume k given by

$$W_k = \frac{E - E_{Tk}}{E - \frac{1-2\nu}{3}E_{Tk}} - \sum_{i=1}^{k-1} W_i \tag{18}$$

where W_k is the weighting factor for sub-volume k and is evaluated sequentially from 1 to the number of sub-volumes N_{sv} and E_{Tk} is the slope of the kth segment of the uniaxial cyclic stress-strain curve. The yield stress for each sub-volume is given by

$$\sigma_{yk} = \frac{1}{2(1-\nu)}[3E\varepsilon_k - (1-2\nu)\sigma_k] \tag{19}$$

where $(\varepsilon_k, \sigma_k)$ is the breakpoint in the uniaxial multi-linear cyclic stress-strain curve. The number of sub-volumes corresponds to the number of breakpoints specified for the definition of the multi-linear stress-strain material relation. Each sub-volume follows the von Mises yield criterion with the associative flow rule and the plastic strain increment for the entire volume is computed according to

$$\Delta\varepsilon_{ij}^{p} = \sum_{k=1}^{N_{sv}} W_k \cdot \Delta\varepsilon_{ij,k}^{p} \tag{20}$$

In the plastic computation algorithm, if the equivalent (von Mises) stress predicted using an elastic trial exceeds the material yield stress given the yield function, then plastic strains will occur. Then a plastic correction will be required, which means that plastic strains reduce the stress state so that it satisfies the yield criterion (return to mapping procedures). The followed scheme for the integration of the elastoplastic constitutive equations consisted of an elastic trial and a return mapping procedure, as proposed by Simo and Taylor [31]. ANSYS commercial code was used in this study with the cyclic plasticity model being already part of the software capabilities [30]. The stabilized cyclic stress-strain curve of the material under consideration in this study is used for the identification of the plasticity constants. In particular, the cyclic stress-strain curve was replaced by a multi-linear representation, the resulting breakpoints being inputted in the model built in the ANSYS commercial code.

4. Probabilistic fatigue damage models

The application of the UniGrow model requires a fatigue damage relation to compute the number of cycles to fail the elementary material blocks. In this section, probabilistic fatigue damage models are proposed rather than the deterministic SWT-*N*, Coffin-Manson or Morrow

http://dx.doi.org/10.5772/64829

models. The probabilistic ε_a-N model proposed by Castillo and Canteli [22] is used. However, since the probabilistic ε_a-N model does not take into account the mean stress effects, a new probabilistic SWT-N field is also proposed, as an extension of the p-ε_a-N field suggested in [22], to include the mean stress influence.

4.1. p-ε-N model

Based on physical and statistical considerations, such as the weakest link principle, stability, limit behaviour, range of the variables and compatibility, Castillo and Canteli [22] derived a probabilistic Weibull model to describe the strain-life field using the same formulation as that proposed by the authors for modelling of the stress-life field. Details of each derivation are found in Castillo et al. [32, 33], where the stress version of the model proves to be successfully applied to different cases of lifetime problems. This leads to the following Weibull strain-life model [33]:

$$p = F\left(N_f^*; \varepsilon_a^*\right) = 1 - exp\left\{-\left[\frac{log\left(N_f/N_0\right)log(\varepsilon_a/\varepsilon_{a0}) - \lambda}{\delta}\right]^{\beta}\right\} \qquad (21)$$
$$log\left(N_f/N_0\right)log(\varepsilon_a/\varepsilon_{a0}) \geq \lambda$$

where p is the probability of failure, N_0 and ε_{a0} are normalizing values, and λ, δ and β are the non-dimensional Weibull model parameters. Their physical meanings (see **Figure 3**) are as follows:

N_0: threshold value of lifetime,

ε_{a0}: endurance limit of ε_a,

λ: parameter defining the position of the corresponding zero-percentile curve,

δ: scale parameter and

β: shape parameter.

Note that the strain-life model (Eq. (21)) has a dimensionless form and reveals that the probability of failure p depends only on the product $N_f^*\varepsilon_a^*$, where $N_f^* = \log\left(N_f/N_0\right)$ and $\varepsilon_a^* = \log\left(\varepsilon_a/\varepsilon_{a0}\right)$, that is

$$N_f^*\varepsilon_a^* \sim W(\lambda, \delta, \beta) \Leftrightarrow N_f^* \sim W\left(\frac{\lambda}{\varepsilon_a^*}, \frac{\delta}{\varepsilon_a^*}, \beta\right) \qquad (22)$$

i.e. $N_f^*\varepsilon_a^*$ follows a Weibull statistical distribution.

This model provides a complete analytical description of the statistical properties of the physical problem being dealt with, including the quantile curves as curves representing the same probability of failure. The model shows, with respect to the conventional strain-life

Coffin-Manson relation, some important advantages. Specifically, it resulted from sound statistical and physical assumptions and not from an empirical arbitrary hypothesis, provides a probabilistic definition of the complete strain-life field without the need of splitting the total strain in its elastic and plastic components but dealing with the total strains directly, includes the run-outs also in the analysis and, finally, also facilitates fatigue damage analysis.

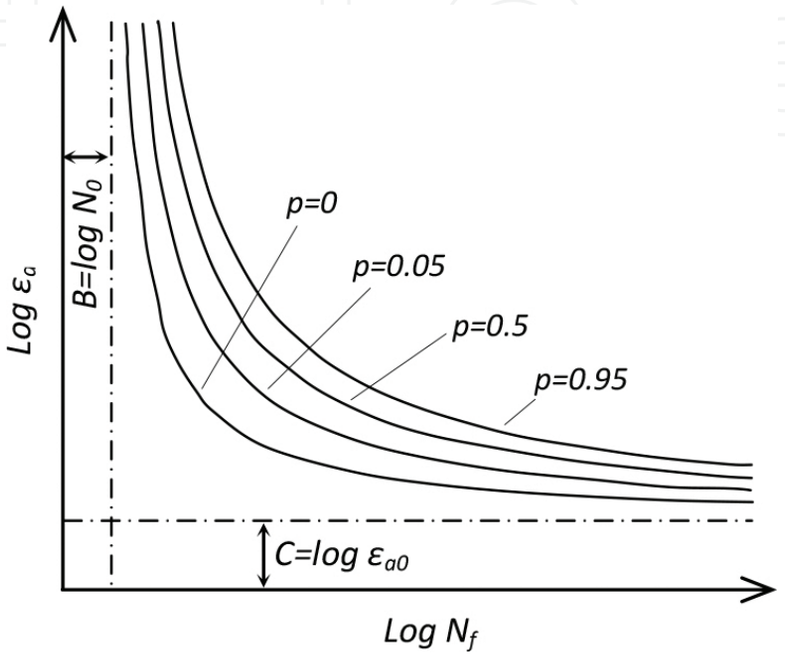

Figure 3. Probabilistic ε_a-N field.

4.2. p-SWT-N model

The SWT (=$\sigma_{max}.\varepsilon_a$) parameter is proposed by Smith et al. [7] in order to take into account the mean stress effects on fatigue life. Any combination of maximum stress and strain amplitude supplying the same value of the SWT parameter should lead to the same fatigue life. The SWT-N and ε_a-N fields exhibit similar characteristics. Therefore, the p-ε-N field proposed by Castillo and Canteli [22] may be extended to represent the p-SWT-N field as

$$p = F\left(N_f^*; SWT^*\right) = 1 - exp\left\{-\left[\frac{log\left(N_f/N_0\right)log(SWT/SWT_0) - \lambda}{\delta}\right]^{\beta}\right\} \qquad (23)$$
$$log\left(N_f/N_0\right)log(SWT/SWT_0) \geq \lambda$$

where p is the probability of failure, N_0 and SWT_0 are normalizing values, and λ, δ and β are the non-dimensional Weibull model parameters. Their physical meanings (see **Figure 4**) are

N_0: threshold value of lifetime and

SWT_0: fatigue limit of SWT,

http://dx.doi.org/10.5772/64829

and the Weibull parameters λ, δ and β with the same meaning as discussed above.

Note that Eq. (23) has a dimensionless form and reveals that the probability of failure p depends only on the product N_f^*SWT*, where $N_f^* = \log\left(N_f/N_0\right)$ and $\text{SWT}^* = \log\left(\text{SWT}/\text{SWT}_0\right)$ that is

$$N_f^* SWT^* \sim W(\lambda, \delta, \beta) \Leftrightarrow N_f^* \sim W\left(\frac{\lambda}{SWT^*}, \frac{\delta}{SWT^*}, \beta\right) \tag{24}$$

i.e. N_f^*SWT* follows a Weibull distribution.

The parameters log N_0 and log ε_{a0} of the p-ε_a-N model, and log N_0 and log SWT_0 of the p-SWT-N model can be estimated by the least square method. The Weibull parameters may be estimated by the maximum likelihood method [32, 33].

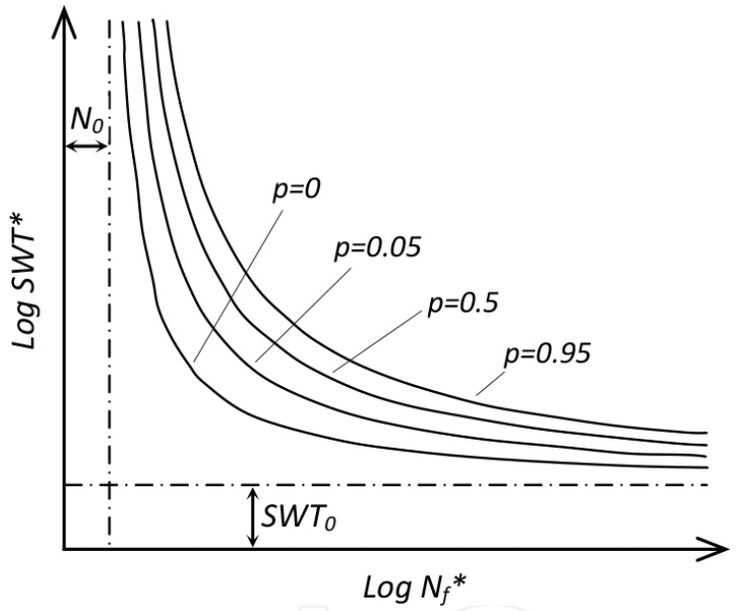

Figure 4. Probabilistic SWT-N_f field.

5. Procedure to generate probabilistic fatigue crack growth rates

A procedure proposed by Correia et al. [34–39] to derive probabilistic fatigue crack propagation fields, based on the UniGrow model, may be summarized into three steps, as follows (see **Figure 5**):

1. Estimation of the Weibull parameters for the p-SWT-N or p-ε_a-N models, described in Section 4, using experimental ε_a-N or SWT-N data from smooth specimens tested under low-cycle fatigue uniaxial tensile loading.

2. Application of the UniGrow model with probabilistic fatigue damage models.

3. Computation of the *p-da/dN-ΔK-R* field.

The UniGrow model is programmed in an Excel workbook, using Visual Basic for Applications (VBA) macros. The problem of the CT specimen geometry was addressed by the code developed [34–39]. The required data are the material properties, loading parameters and geometric dimensions of the CT specimen, including the initial and final crack sizes to be simulated. Also, the elementary material element size, ρ^*, is an input that after the first trial may be iteratively corrected to result in a satisfactory fit between the experimental and numerical data. **Figure 3** gives a general overview of the procedure.

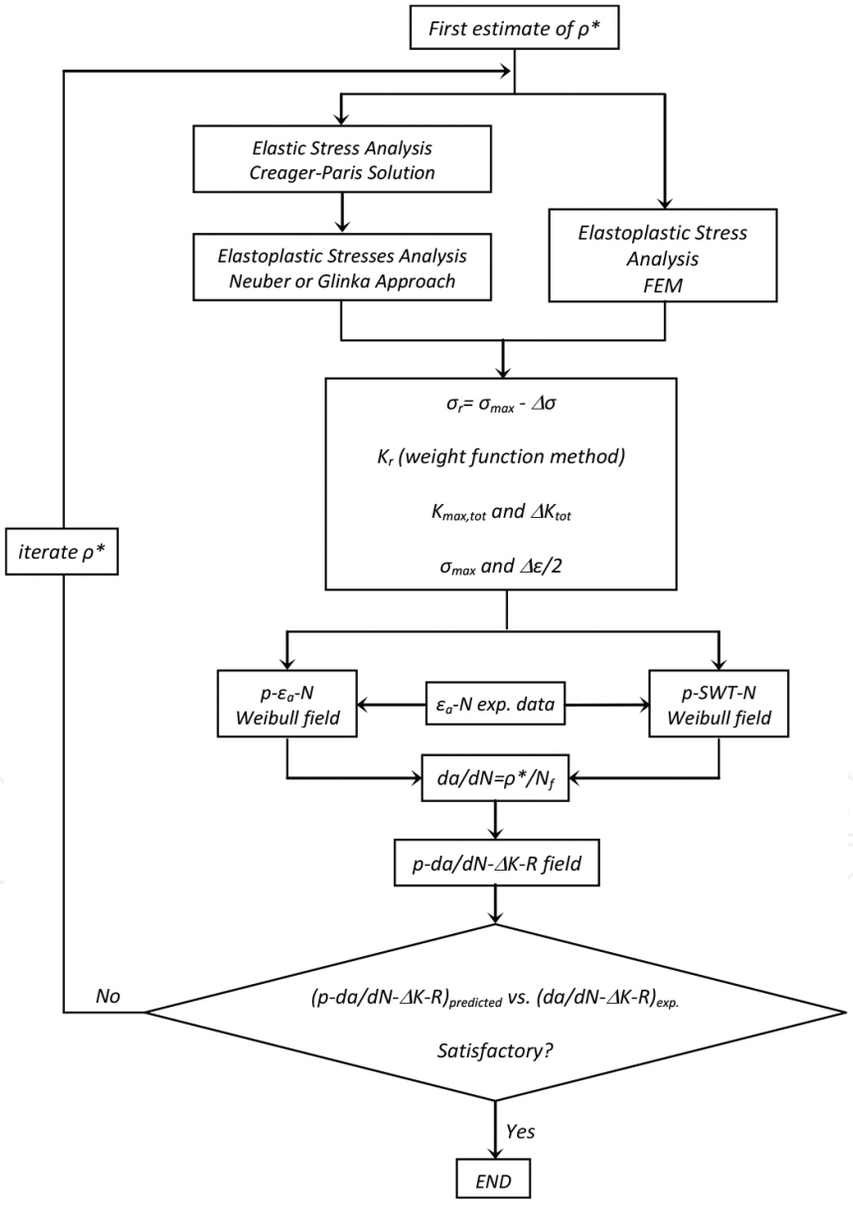

Figure 5. Procedure to generate probabilistic fatigue crack propagation fields.

http://dx.doi.org/10.5772/64829

Neuber and Glinka's approaches for the elastoplastic analysis are both possible to be applied to the cracked CT specimen [15, 25] and a multi-axial elastoplastic calculation as suggested by Moftakhar et al. [16] and Reinhard et al. [17] are programmed. This multi-axial approach is supported by Hencky's total deformation equations that proved to yield reliable predictions for the stress-strain field at notched details under proportional loading. Besides the crack tip material element analysis, the UniGrow model also requires the computation of the elastoplastic stress-strain response along the crack path, in order to facilitate the residual stress assessment. However, the above referred analytical multi-axial elastoplastic approaches are not able to model the stress redistribution due to yielding, which may lead to inconsistent predictions of the residual stresses. To overcome this limitation of the analytical approaches, in this research the residual stresses are computed preferably using an elastoplastic finite-element approach, the results being verified against those coming from the referred analytical solutions. The residual stresses play a central role in the UniGrow model; therefore, the accuracy of the residual stress evaluation method is vital for attaining consistent fatigue crack growth rate predictions.

The probabilistic fatigue crack propagation fields are alternatively assessed using the probabilistic ε_a-N and SWT-N fields. For each fatigue damage model, independent material element sizes, ρ^*, are identified and compared.

6. Basic fatigue data of the P355NL1 steel

The P355NL1 steel is a pressure vessel steel, the fatigue behaviour of which has been already analysed [21, 35, 39, 40]. This section presents the cyclic elastoplastic fatigue data and the fatigue crack growth data obtained for the P355NL1 steel [21]. The strain-life behaviour of the P355NL1 steel is evaluated through fatigue tests of smooth specimens, carried out under strain-controlled conditions, according to the ASTM E606 standard [41]. Two series of specimens, 19 and 24 specimens, are tested under distinct strain ratios, $R_\varepsilon = 0$ and –1, respectively. The cyclic Ramberg-Osgood [42] and Morrow [6] strain-life parameters of the P355NL1 steel are summarized in **Table 1**, for the conjunction of both strain ratios [21, 35, 39, 40]. The Ramberg-Osgood properties are represented by the cyclic strain hardening coefficient, K' and the cyclic strain exponent, n'. The fatigue ductility coefficient ε_f', the fatigue ductility exponent c, the fatigue strength coefficient σ_f' and the fatigue strength exponent b are parameters of the Morrow strain-life relation. The elastic and monotonic tensile properties of this pressure vessel steel under investigation, as represented by the Young modulus E, Poisson ratio ν, the ultimate tensile strength f_u and upper yield stress f_y, are shown in **Table 2**.

Material	σ'_f	b	ε'_f	c	K'	n'
	MPa	–	–	–	MPa	–
P355NL1	1005.50	−0.1033	0.3678	−0.5475	948.35	0.1533

Table 1. Cyclic elastoplastic and strain-life properties of the P355NL1 steel, $R_\varepsilon = -1$ and $R_\varepsilon = 0$.

Material	E	v	f_v	f_y
	GPa	–	MPa	MPa
P355NL1	205.20	0.275	568.11	418.06

Table 2. Elastic and tensile properties of the P355NL1 steel.

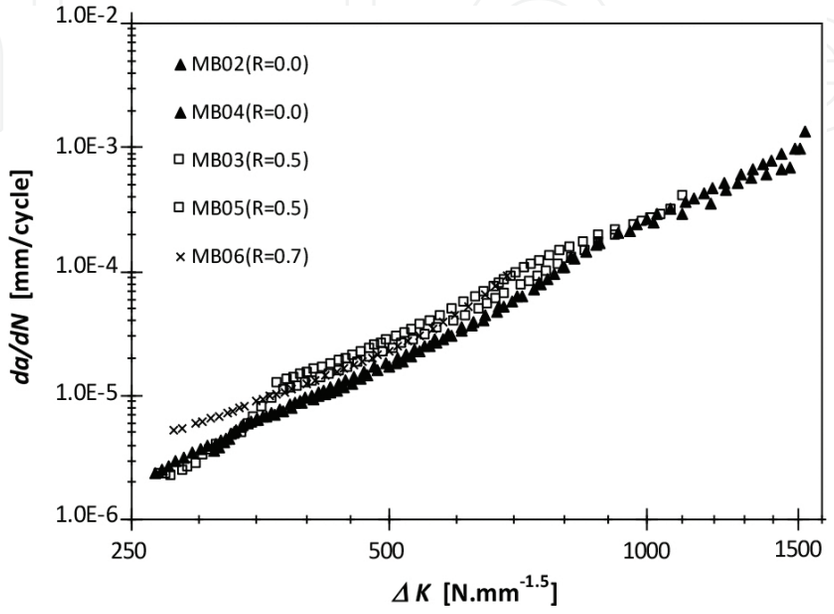

Figure 6. Fatigue crack propagation data obtained for the P355NL1 steel.

Fatigue crack growth rates of the investigated materials are also evaluated for several stress R-ratios, using CT specimens, following the recommendations of the ASTM E647 standard [43]. The CT specimens of P355NL1 steel are defined with a width, $W = 40$ mm and a thickness, $B = 4.5$ mm [21, 35, 39, 40]. All tests are performed in air, at room temperature, under a sinusoidal waveform at a maximum frequency of 20 Hz. The crack growth data derived for the P355NL1 steel, for three tested stress ratios, $R_\sigma = 0.0$, $R_\sigma = 0.5$ and $R\sigma = 0.7$, are illustrated in **Figure 6**. The crack propagation rates are only slightly influenced by the stress ratio. Higher stress ratios provide higher crack growth rates. **Figures 7** and **8** show the p-SWT-N and p-ε_a-N fields, respectively, which are identified for the P355NL1 pressure vessel steel, using the experimental data from the fatigue tests on smooth specimens. The constants of the Weibull fields are also shown in the figures, in particular the threshold constants (B and C) and the Weibull parameters (β, λ and δ). The extrapolations using the Weibull field should be avoided mostly for very low-cycle fatigue regimes. It is verified in this study that the number of cycles to fail the material's representative element, in the fatigue crack propagation regime II, is generally in the low- to very low-cycle fatigue regimes. Thus, it is decided to enhance the Weibull field in this region postulating some fatigue data at the low- to very low-cycle fatigue regimes, using the available deterministic Morrow's equation. The Morrow's equation does not show the vertical asymptote as verified with the Weibull field, being physically more consistent when performing extrapolations for very low number of cycles.

http://dx.doi.org/10.5772/64829

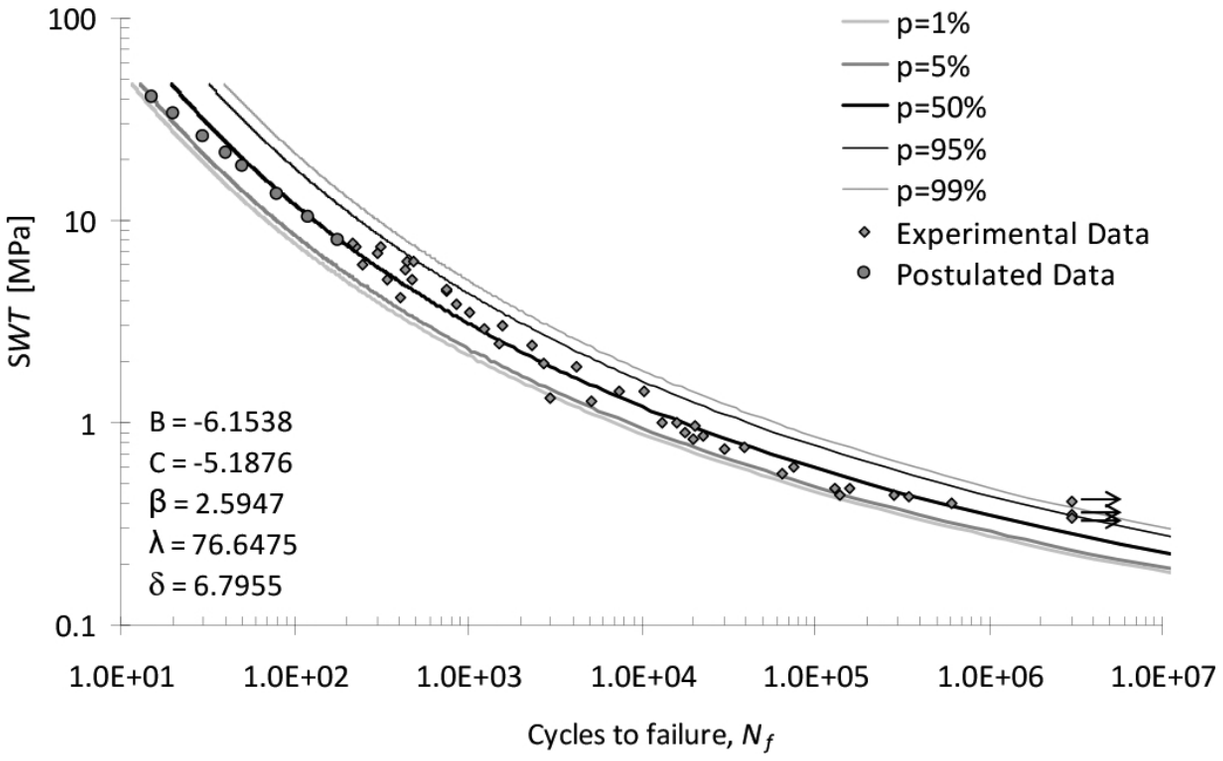

Figure 7. *p*-SWT-*N* field for the P355NL1 steel.

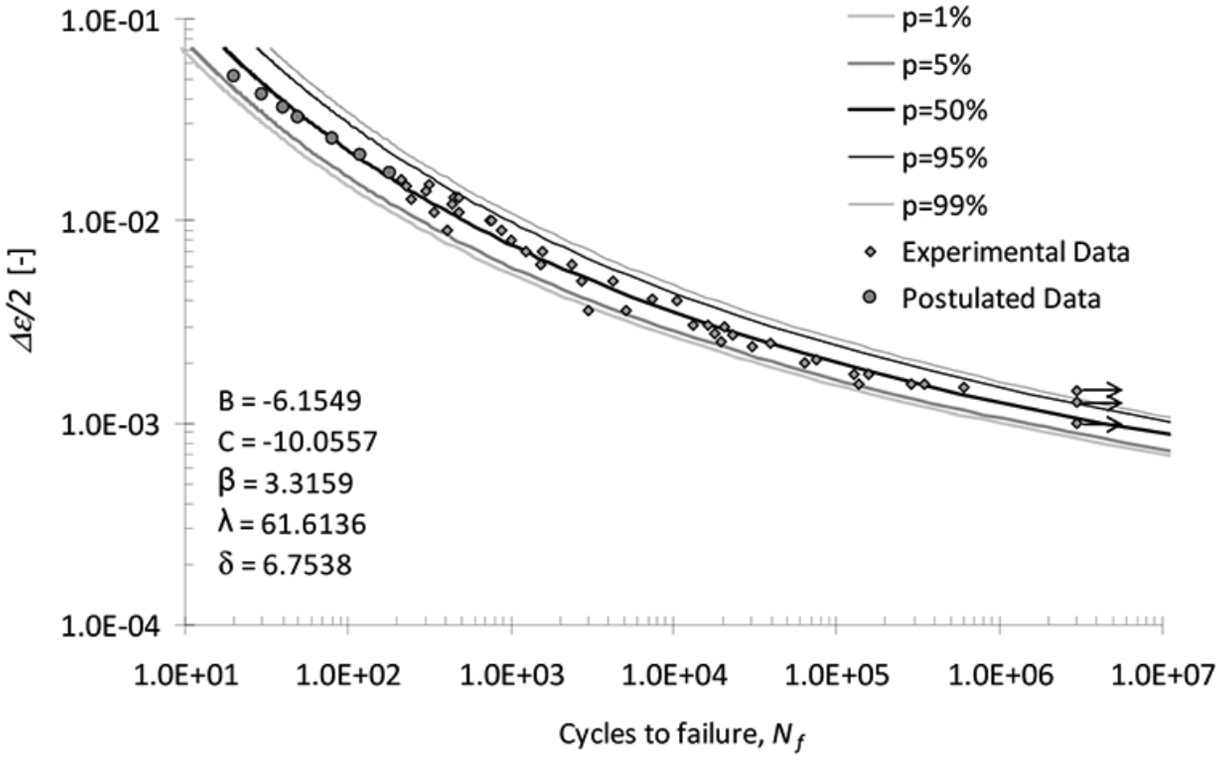

Figure 8. *p*-ε_a-*N* field for the P355NL1 steel.

7. Prediction of the probabilistic fatigue crack propagation fields

The prediction of the probabilistic fatigue crack propagation fields is performed through the application of the UniGrow model to CT specimens. Additionally, the elementary material block size, ρ^*, is required and is evaluated by a trial and error procedure in order to achieve good agreement between the predicted and experimental da/dN versus ΔK data, for the P355NL1 steel under consideration. The probabilistic fatigue crack propagation fields are evaluated using, alternatively, the probabilistic p-ε_a-N and p-SWT-N fields (see procedure described in Section 6).

7.1. Numerical FE simulation of the compact tension specimens

Two-dimensional numerical models of the CT specimens are developed using nonlinear elastoplastic finite-element modelling. These models were useful to assess the accuracy of residual stress estimation using the simplified elastoplastic analysis. A very refined finite-element mesh at the crack tip region is used to model conveniently the crack tip geometry with a notch radius, ρ^* (refer to **Figure 1b** for geometric details). **Figure 9** illustrates the finite-element mesh of the CT specimen along with the respective boundary conditions. One-half of the geometry is modelled, taking advantage of the existing symmetry. 2D plane stress elements are used since the specimens' thickness is relatively thin (B = 4.5 mm for the P355NL1 steel).

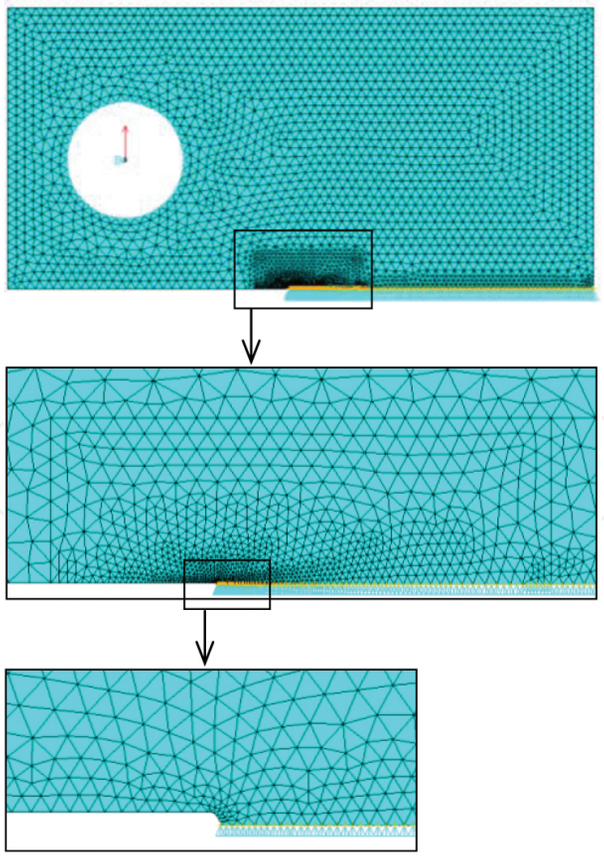

Figure 9. Typical finite-element mesh of the CT specimen.

http://dx.doi.org/10.5772/64829

Quadratic triangular elements (six-noded elements) are selected and applied with a full integration formulation. The pin loading used in the CT testing is simulated with a rigid-to-flexible frictionless contact, the pin being modelled as a rigid circle controlled by a pilot node.

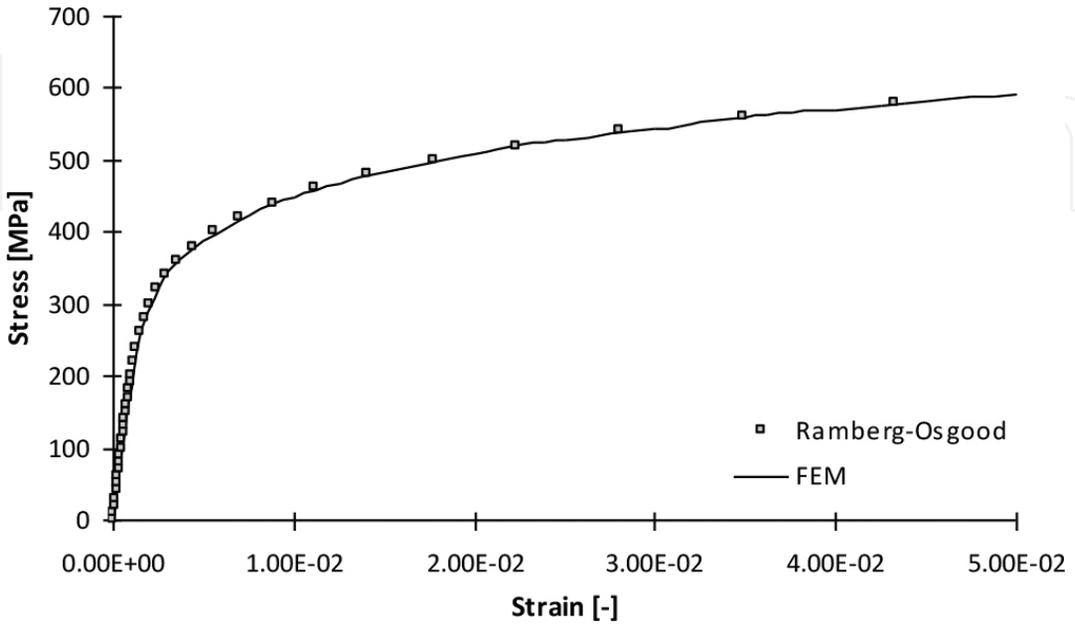

Figure 10. Cyclic stress-strain relation obtained for the P355NL1 steel [39].

Maximum stresses	Mesh 5	Mesh 4	Mesh 1	Mesh 2	Mesh 3
σ_y **(MPa)**	1367.9	1420.1	1495.8	1605.3	1606.7
***Dev*. (%)**	−14.79	−11.54	−6.82	–	0.09
σ_x **(MPa)**	347.4	370.3	363.9	354.2	354.1
***Dev*. (%)**	−1.93	4.57	2.74	–	−0.03

Table 3. Maximum elastic stresses for distinct finite-element mesh densities for the P355NL1 steel (F_{max} = 1634.1 N, ρ^* = 30 Âμm).

All numerical simulations are carried out using the ANSYS® 12.0 code [30]. The six-noded plane element adopted in the finite-element analyses is the PLANE181 element available in the ANSYS® 12.0 code library. The contact and target elements used in the pin-loading simulation are, respectively, the CONTA172 and TARGE169 elements available in ANSYS® 12.0 code [30]. A parametric model is built using the APDL language. The surface of the holes is modelled as flexible using CONTA172 elements. The augmented Lagrangian contact algorithm is used. The associative von Mises (J2) yield criterion with multi-linear kinematic hardening is used to model the plastic behaviour. The multi-linear kinematic hardening uses the Besseling model, also called the sub-layer or overlay model, so that the Bauschinger effect is included. The plasticity model was fitted to the stabilized or half-life pseudo-stabilized cyclic

curve of the materials. The von Mises yield criterion with multi-linear kinematic hardening is adopted to model the plastic behaviour.

The finite-element model is initially applied to perform elastic and elastoplastic stress analyses in order to allow us the comparison between the elastic and elastoplastic stress distributions as resulting from the Creager-Paris solution [24] and the multi-axial Neuber approach [15], respectively.

One important assumption of the UniGrow model consists in applying the compressive residual stresses that are computed ahead of the crack tip, in the crack faces, in a symmetric way with respect to the normal to crack face that passes through the crack tip. The resulting residual stress intensity factor K_r is computed using the weight function method [26], for each of the stress ratios covered by the testing program.

Figures 9 and **10** show the finite-element mesh of the CT geometry and the cyclic stress-strain curves adopted in the plasticity model of the P355NL1 steel, respectively [39]. The Ramberg-Osgood relation [42] is compared with the response of the finite-element model reproducing a uniaxial stress state in **Figure 10**. **Table 3** presents the maximum elastic stresses (σ_x and σ_y) ahead of the crack tip, resulting from distinct mesh densities illustrated in **Figure 11**. The mesh 2 is adopted for residual stress computation. Results presented in **Table 3** compare the mesh 2 with the other meshes.

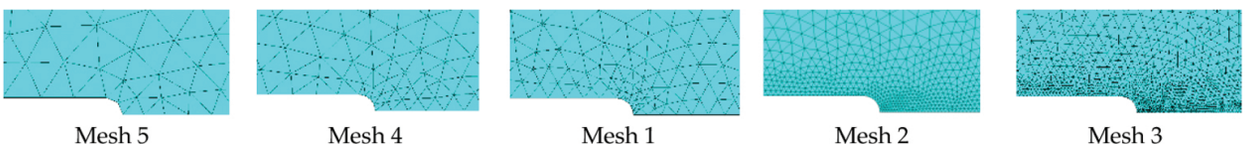

Figure 11. Finite-element meshes used in the convergence study performed for the CT specimen.

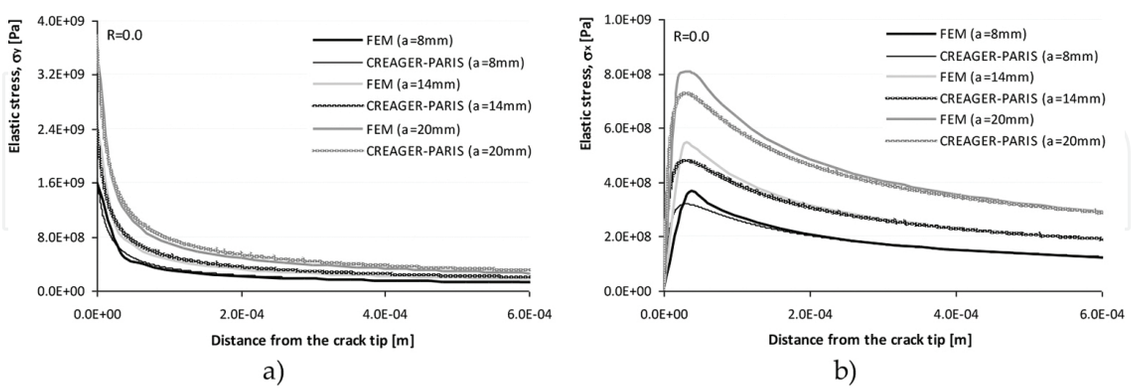

Figure 12. Comparison between analytical and numerical results of the elastoplastic stress distribution ahead of the crack tip and along the crack line ($y = 0$) for CT specimens made of the P355NL1 steel (F_{max} = 1643.1 N, ρ^* = 30 μm): (a) σ_y stress distribution and (b) σ_x stress distribution.

Figures 12 and **13** illustrate the elastic and elastoplastic stress distributions for the P355NL1 steel, respectively. In these figures, the numerical and analytical solutions for the CT specimens

http://dx.doi.org/10.5772/64829

are computed for a crack tip radius, $\rho^* = 30$ μm, which is found to be the best value for the P355NL1 steel. This ρ^* parameter gives the best predictions of the fatigue crack growth rates, using the Morrow relation as referred in [6]. **Figure 14** shows the residual stress distributions for the P355NL1 steel for distinct crack sizes and stress *R*-ratios. The residual stress distributions are computed by means of the analytical and numerical solutions using an elementary material block size, $\rho^* = 30$ μm [39]. **Figure 15** illustrates the stress and strain fields along the *y*- (load) direction obtained for the CT specimens using the elastoplastic finite-element analysis and the properties of the P355NL1 steel, for a material's representative element $\rho^* = 30$ μm, a crack size $a = 14$ mm, a maximum load $F_{max} = 1634.1$ N and a stress *R*-ratio $R_\sigma = 0.0$. The stress and strain fields are shown at the end of the first loading reversal and at the end of the first unloading reversal. **Figure 16** presents the residual stress intensity factor range for an elementary material block size $\rho^* = 30$ μm [39] as a function of the applied stress intensity factor range obtained with the numerical analysis.

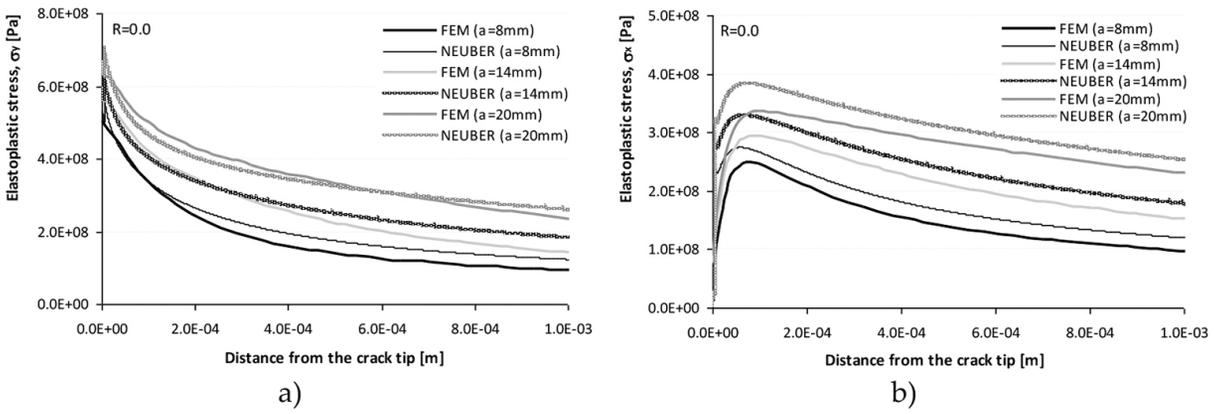

Figure 13. Comparison between analytical and numerical results of the elastoplastic stress distribution ahead of the crack tip and along the crack line ($y = 0$) for CT specimens made of the P355NL1 steel ($F_{max} = 1643.1$ N, $\rho^* = 30$ μm): (a) σ_y stress distribution and (b) σ_x stress distribution.

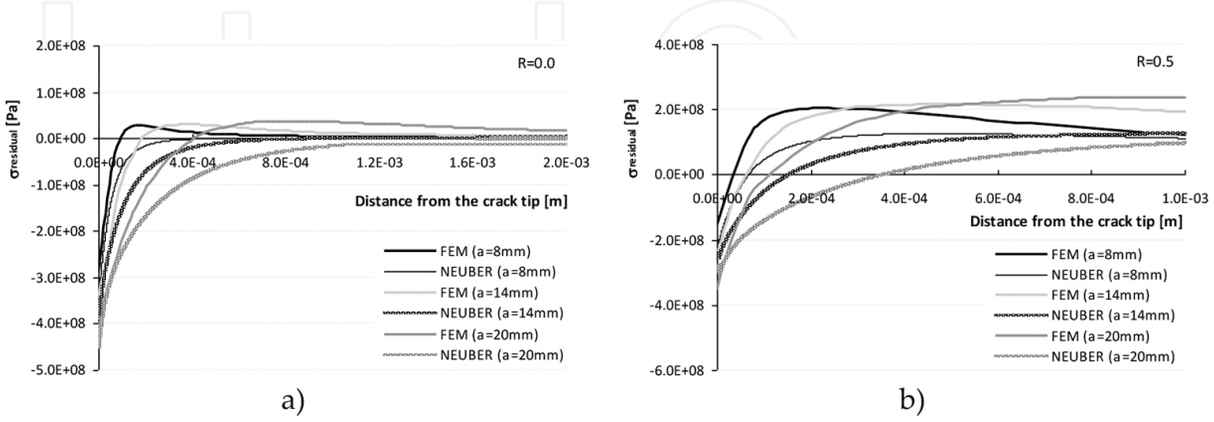

Figure 14. Comparison between analytical and numerical results of the residual stress distribution ahead of the crack tip and along the crack line ($y = 0$) for CT specimens made of the P355NL1 steel ($F_{max} = 1643.1$ N, $\rho^* = 30$ μm).(a) $R_\sigma = 0.0$ and (b) $R_\sigma = 0.5$.

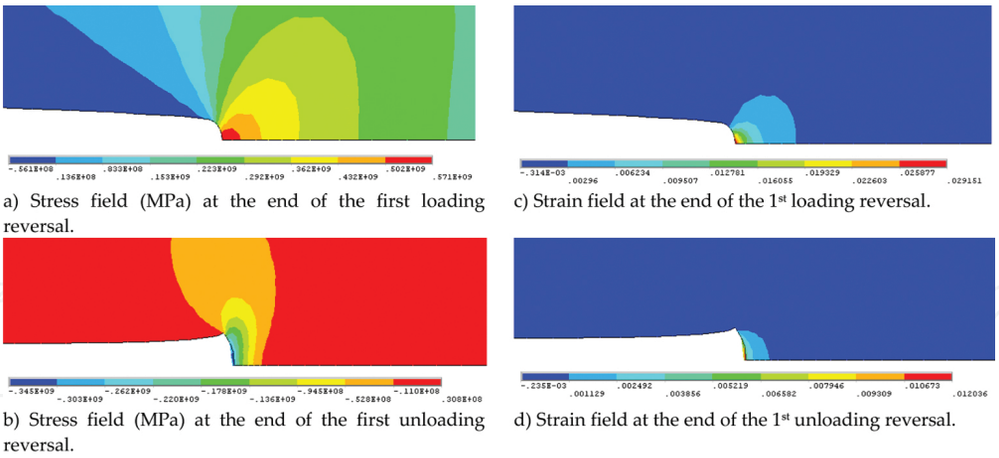

a) Stress field (MPa) at the end of the first loading reversal.

c) Strain field at the end of the 1st loading reversal.

b) Stress field (MPa) at the end of the first unloading reversal.

d) Strain field at the end of the 1st unloading reversal.

Figure 15. Stress and strain fields for the load direction, obtained for the CT geometries made of P355NL1 steel, resulting from elastoplastic finite-element analysis (F_{max} = 1634.1 N, ρ^* = 30 μm, a = 14 mm, R_σ = 0.0). (a) Stress field (MPa) at the end of the first loading reversal. (b) Stress field (MPa) at the end of the first unloading reversal. (c) Strain field at the end of the first loading reversal. (d) Strain field at the end of the first unloading reversal.

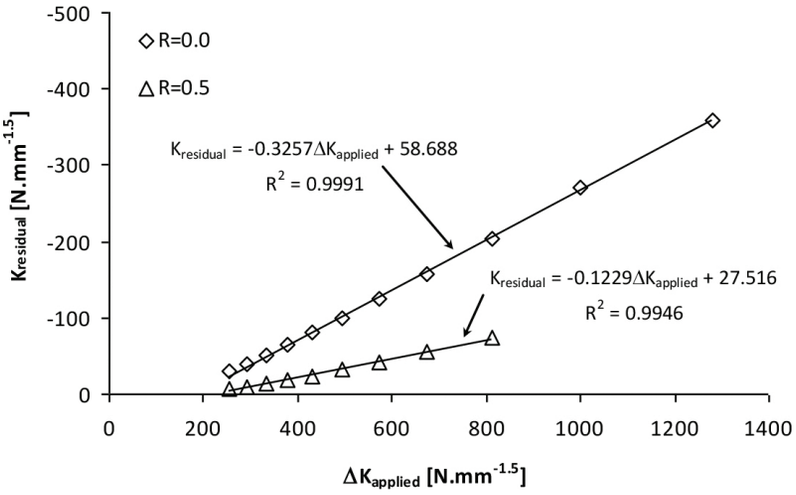

Figure 16. Residual stress intensity factor as a function of the applied stress intensity factor range.

The elastic stress distribution sustains a very good agreement between the analytical and numerical results, for several crack sizes, within a small distance from the crack tip. The analytical solutions lead to higher maximum absolute stresses than the elastoplastic FE analysis. The analytical solution does not show plastic zone behaviour, which is a clear limitation of the analytical approach. The increasing of the stress ratio affects the compressive residual stresses that decrease progressively with increasing stress ratio. This trend is responsible for increasing the effectiveness of the applied stress intensity range as a crack driving force. The extension of the compressive residual stresses increases for higher crack lengths. The numerical compressive stress region is always lower than the one obtained by the analytical analysis. Therefore, the numerical solution, for the residual stresses, is adopted in the crack propagation prediction, based on the UniGrow model. A very high linear correlation

http://dx.doi.org/10.5772/64829

between the residual stress intensity factor and the applied stress range is verified for each stress *R*-ratio. This linear relation agrees with the proposition by Noroozi et al. [12] based on analytical analysis.

7.2. Results and discussion

Finally, in this section, the UniGrow model is applied to compute the fatigue crack propagation rates for the same fatigue crack propagation data described in Section 6. As detailed before, the residual stress intensity factor is calculated using a compressive residual stress distribution computed from numerical analysis and the weight function technique [26]. The strain range and maximum stress, needed by the probabilistic strain-life or SWT-life fields, are evaluated using an analytical calculation applied over the first material element ahead of the crack tip, keeping the original structure of the UniGrow model. Average strain and stress values, along the first elementary material block, are used instead of peak values. The analytical solution produces reliable results at the crack tip notch root as verified in previous section. The original structure of the UniGrow model presents some advantages: (i) provides a direct correspondence with fracture mechanics based analyses, which facilitates the physical understanding of the process, (ii) allows close-form solutions for fatigue crack propagation laws to be achieved in the same format as that of existing fracture mechanics approaches and (iii) requires inexpensive computations.

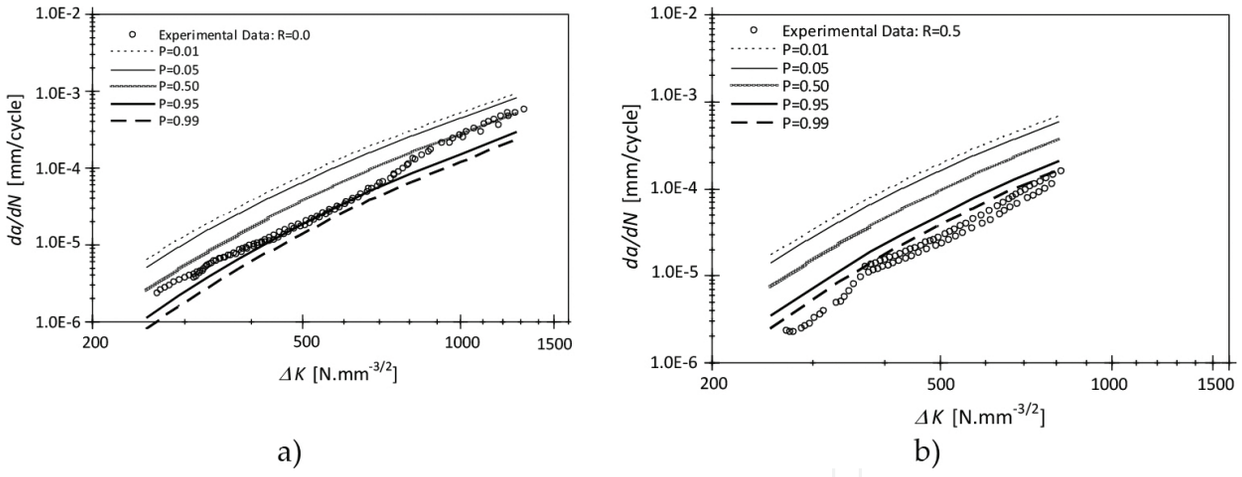

Figure 17. Probabilistic prediction of the fatigue crack propagation based on the *p*-SWT-*N* field for the P355NL1 steel ($\rho^* = 3 \times 10^{-5}$ m): (a) $R_\sigma = 0.0$ and (b) $R_\sigma = 0.5$.

The probabilistic ε_a-*N* and SWT-*N* fields are used to derive the probabilistic fatigue crack propagation fields (*p*-*da*/*dN*-Δ*K*-*R* fields). For each case, an independent identification of the elementary material block size, ρ^*, is performed. **Figure 17** shows the probabilistic fatigue crack propagation fields obtained for the P355NL1 steel, using the *p*-SWT-*N* material fields. **Figure 18** illustrates the probabilistic fatigue crack propagation fields predicted for the P355NL1 steel, resulting from the *p*-ε_a-*N* material fields.

Elementary material block size of 3×10^{-5} m is found adequate for the P355NL1 steel, resulting from the application of the *p*-ε-*N* fields. The elementary material block size found for the P355NL1 steel is higher than those proposed by Noroozi et al. [13] for the 4340 steel ($\rho^* = 2 \times 10^{-6}$ m). So far, there are no conclusive studies relating the micro-structural grain sizes with the elementary material block sizes. Nevertheless, it can be anticipated that ρ^* can be indirectly dependent on the micro-structural features of the analysed material (e.g. grain size) but it cannot be uniquely associated with any specific micro-structural particle size. Therefore, the material grain size may be considered just one of the possible micro-structural features affecting the definition of ρ^*.

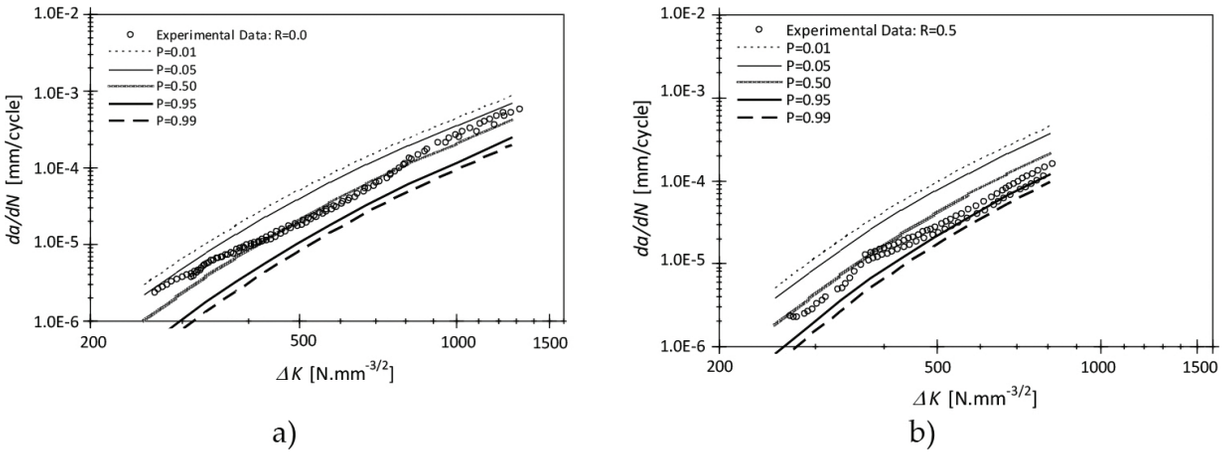

Figure 18. Probabilistic prediction of the fatigue crack propagation based on the *p*-ε_a-*N* field for the P355NL1 steel ($\rho^* = 3 \times 10^{-5}$ m): (a) $R_\sigma = 0.0$ and (b) $R_\sigma = 0.5$.

Concerning the probabilistic fatigue crack propagation rate fields of the P355NL1 steel, it is clear that the use of the *p*-SWT-*N* model overestimates the effects of the stress *R*-ratio. Using the probabilistic SWT-*N* model, the stress ratio effects are accounted twice, through the residual stress intensity factor (compressive residual stresses effects) and through the mean stress of the cycle. Nevertheless, the number of cycles required to crack the material element fall within the very low- to low-cycle fatigue regimes at which a rapid cyclic mean stress relaxation is verified. However, the multi-linear kinematic hardening model used in the investigation is not capable of simulating the cyclic mean stress relaxation. The predictions based on the *p*-ε_a-*N* model are satisfactory. First, they define lower and upper bounds for the available experimental data. Secondly, the major influence of the stress ratio is verified when it changes from 0 to 0.5. In the damage computations presented in the chapter, the prior loading history on crack tip elements is not considered. Preliminary calculations performed considering the prior loading history on a set of elements ahead of the crack tip, forming a process zone, show only a marginal influence on *da*/*dN* predictions, mainly in the propagation regimes I and II. Nonetheless, the computational costs associated to simultaneous damaged elements increases very significantly.

8. Conclusions

An assessment of the UniGrow model is presented in this chapter, based on available experimental data for the P355NL1 steel under consideration. The UniGrow model is also extended to predict probabilistic fatigue crack propagation fields, replacing the deterministic SWT-*N* relation proposed in the original UniGrow model by the *p*-SWT-*N* or *p*-ε_a-*N* fields. In the present chapter, the *p*-SWT-*N* field is first proposed as a generalization of the *p*-ε_a-*N* field, in order to take into account the mean stress effects. Both *p*-SWT-*N* and *p*-ε_a-*N* fields led to satisfactory correlations of the experimental data available for the P355NL1 steel under investigation.

The multi-axial analytical Neuber elastoplastic analysis proposed in the UniGrow model to compute the residual stress distribution is assessed using elastoplastic finite-element analysis. Inconsistent compressive residual stress distributions, mainly for $R_\sigma = 0$, are found using this approach. The multi-axial Neuber model does not take into account stress redistribution due to yielding and therefore does not provide the dimensions of the plastic zone. The residual compressive stress intensity factor, computed with the compressive residual stress field from the finite-element analysis, exhibits a linear relation with the applied stress intensity factor range, which confirms the typical trend documented in literature of linear increase of the residual stress intensity factor with the applied stress intensity factor range, for a specific stress *R*-ratio.

The *p*-*da*/*dN*-Δ*K*-*R* fields predicted for the P355NL1 steel, based on material *p*-ε_a-*N* field, produce satisfactory results, since this material shows crack propagation rates with relatively small sensitivity to the stress *R*-ratio. The elementary material block size for the P355NL1 steel is found to be about one order of magnitude higher than the value proposed by Noroozi et al. [14] for the 4340 steel. The ρ^* can be indirectly dependent on the micro-structural features of the analysed material (e.g. grain size) but it cannot be uniquely associated with any specific micro-structural particle size.

Acknowledgements

The authors acknowledge the Portuguese Science Foundation (FCT) for the financial support through the postdoctoral grant SFRH/BPD/107825/2015. The authors gratefully acknowledge the funding of SciTech: Science and Technology for Competitive and Sustainable Industries, R&D project co-financed by Programa Operacional Regional do Norte (NORTE2020), through Fundo Europeu de Desenvolvimento Regional (FEDER). Dr. Moreira acknowledges Programa Operacional Potencial Humano (POPH), Quadro de Referência Estratégico Nacional (QREN)-Tipologia 4.2 promotion of scientific employment funded by the European Social Fund (ESF) and Ministério da Ciência, Tecnologia e Ensino Superior (MCTES).

Author details

José António Fonseca De Oliveira Correia[1*], Abílio M.P. De Jesus[1], Pedro M.G.P. Moreira[1], Rui A.B. Calçada[1] and Alfonso Fernández-Canteli[2]

*Address all correspondence to: jacorreia@inegi.up.pt

1 Faculty of Engineering, University of Porto, Porto, Portugal

2 Department of Construction and Manufacturing Engineering, University of Oviedo, Gijón, Spain

References

[1] Schütz W. A history of fatigue. Eng. Fract. Mech., 1996; 54: 263–300.

[2] Paris PC, Gomez M, Anderson WE. A rational analytic theory of fatigue. Trend Engineering, 1961; 13: 9–14.

[3] Beden SM, Abdullah S, Ariffin AK. Review of fatigue crack propagation models for metallic components. European Journal of Scientific Research, 2009; 28: 364–397.

[4] Coffin LF. A study of the effects of the cyclic thermal stresses on a ductile metal. Trans ASME, 1954;76:931–50.

[5] Manson SS. Behaviour of materials under conditions of thermal stress, NACA TN-1170, National Advisory Committee for Aeronautics, 1954; Report 1170, pp. 591–630. http://naca.central.cranfield.ac.uk/reports/1954/naca-report-1170.pdf

[6] Morrow JD. Cyclic plastic strain energy and fatigue of metals. Int Frict Damp Cyclic Plast ASTM STP., 1965; 378:45–87.

[7] Smith KN, Watson P, Topper TH. A stress-strain function for the fatigue of metals. Journal of Materials, 1970; 5(4): 767–778.

[8] Shang D-G, Wang D-K, Li M, Yao W-X. Local stress–strain field intensity approach to fatigue life prediction under random cyclic loading. International Journal of Fatigue, 2001; 23: 903–910.

[9] Glinka G. A notch stress-strain analysis approach to fatigue crack growth. Engineering Fracture Mechanics, 1985; 21: 245–261.

[10] Peeker E, Niemi E. Fatigue crack propagation model based on a local strain approach. Journal of Constructional Steel Research, 1999; 49: 139–155.

[11] Noroozi AH, Glinka G, Lambert S. A two parameter driving force for fatigue crack growth analysis. International Journal of Fatigue, 2005; 27: 1277–1296.

[12] Noroozi AH, Glinka G, Lambert S. A study of the stress ratio effects on fatigue crack growth using the unified two-parameter fatigue crack growth driving force. International Journal of Fatigue, 2007; 29:1616–1633.

[13] Noroozi AH, Glinka G, Lambert S. Prediction of fatigue crack growth under constant amplitude loading and a single overload based on elasto-plastic crack tip stresses and strains. Engineering Fracture Mechanics, 2008; 75: 188–206.

[14] Hurley PJ, Evans WJ. A methodology for predicting fatigue crack propagation rates in titanium based on damage accumulation. Scripta Materialia, 2007; 56: 681–684.

[15] Neuber H. Theory of stress concentration for shear-strained prismatic bodies with arbitrary nonlinear stress–strain law. Transactions of ASME Journal of Applied Mechanics, 1961; 28: 544–551.

[16] Moftakhar A, Buczynski A, Glinka G. Calculation of elasto-plastic strains and stresses in notches under multiaxial loading. International Journal of Fracture, 1995; 70: 357–373.

[17] Reinhard W, Moftakhar A, Glinka G. An efficient method for calculating multiaxial elasto-plastic notch tip strains and stresses under proportional loading. Fatigue and Fracture Mechanics, ASTM STP 1296, Piascik RS, Newman JC, Dowling NE, Eds., American Society for Testing and Materials, 1997; 27: 613–629.

[18] Mikheevskiy S, Glinka G. Elastic–plastic fatigue crack growth analysis under variable amplitude loading spectra. International Journal of Fatigue, 2009; 31: 1828–1836.

[19] De Jesus AMP, Silva ALL, Figueiredo MV, Correia JAFO, Ribeiro AS, Fernandes AA. Strain-life and crack propagation fatigue data from several Portuguese old metallic riveted bridges. Engineering Failure Analysis, 2010; 17: 1495–1499.

[20] De Jesus AMP, Matos R, Fontoura BFC, Rebelo C, Simões da Silva L, Veljkovic M. A comparison of the fatigue behaviour between S355 and S690 steel grades. Journal of Constructional Steel Research, 2012; 79: 140–150.

[21] De Jesus AMP, Ribeiro AS, Fernandes AA. Influence of the submerged arc welding in the mechanical behaviour of the P355NL1 steel—Part II: Analysis of the Low/High Cycle Fatigue Behaviours. J. Mater. Sci., 2007; 42: 5973–5981.

[22] Castillo E, Fernández-Canteli A. A Unified Statistical Methodology for Modeling Fatigue Damage. Springer, Netherlands, 2009; 232.

[23] Basquin OH. The exponential law of endurance tests. Proc. Annual Meeting American Society for Testing Materials, 1910; 10: 625–630.

[24] Creager M, Paris PC. Elastic field equations for blunt cracks with reference to stress corrosion cracking. International Journal of Fracture Mechanics, 1967; 3: 247–252.

[25] Molski K, Glinka G. A method of elastic-plastic stress and strain calculation at a notch root. Materials Science and Engineering, 1981; 50: 93–100.

[26] Glinka G. Development of weight functions and computer integration procedures for calculating stress intensity factors around cracks subjected to complex stress fields. Progress Report No. 1: Stress and Fatigue-Fracture Design, Petersburg, Ontario, Canada, 1996; 108. http://www.afgrow.net/downloads/documents/SaFFD_1m.pdf

[27] Sadananda K, Vasudevan AK, Kang IW. Effect of superimposed monotonic fracture modes on the ΔK and Kmax parameters of fatigue crack propagation. Acta Materialia, 2003; 51(22): 3399–3414.

[28] Kajawski D. A new (ΔK+Kmax)0.5 driving force parameter for crack growth in aluminium alloys. International Journal of Fatigue, 2001; 23(8): 733–740.

[29] Schiffner K. Overlay models for structural analysis under cyclic loading. Computers and Structures, 1995; 56(2/3): 321–328.

[30] SAS, Version 12.0, ANSYS, Swanson Analysis Systems, Inc., Houston, 2011.

[31] Simo JC, Taylor RL. Consistent tangent operators for rate-independent elastoplasticity. Computer Methods in Applied Mechanics and Engineering, 1985; 48: 101–118.

[32] Castillo E, Galambos J. Lifetime regression models based on a functional equation of physical nature. Journal of Applied Probability, 1987; 24: 160–169.

[33] Castillo E, Fernández-Canteli A, Hadi AS, López-Anelle M. A Fatigue Model with Local Sensitivity Analysis, Fatigue and Fracture of Engineering Material and Structure, 2006; 30: 149–168.

[34] Correia JAFO, De Jesus AMP, Fernández-Canteli A. A procedure to derive probabilistic fatigue crack propagation data. International Journal of Structural Integrity, 2012; 3(2): 158–183.

[35] Correia JAFO, De Jesus AMP, Fernández-Canteli A. Local unified model for fatigue crack initiation and propagation: application to a notched geometry. Engineering Structures, 2013; 52: 394–407.

[36] Correia JAFO. An integral probabilistic approach for fatigue lifetime prediction of mechanical and structural components. Ph.D. Thesis, University of Porto, 2014; p. 382.

[37] Correia JAFO, De Jesus AMP, Fernández-Canteli A, Calçada RAB. Modelling probabilistic fatigue crack propagation rates for a mild structural steel. Frattura ed Integrita Strutturale, 2015; 31: 80–96.

[38] Hafezi MH, Abdullah NN, Correia JAFO, De Jesus AMP. An assessment of a strain-life approach for fatigue crack growth. International Journal of Structural Integrity, 2012; 3(2): 344–376.

[39] De Jesus AMP, Correia JAFO. Critical assessment of a local strain-based fatigue crack growth model using experimental data available for the P355NL1 steel. Journal of Pressure Vessel Technology, 2013; 135(1): 011404-1–0114041-9.

[40] Correia JAFO, De Jesus AMP, Moreira PMGP, Tavares PJ. Crack closure effects on fatigue crack propagation rates: application of a proposed theoretical model. Advances in Materials Science and Engineering, 2016: (2016), Article ID 3026745, 11. http://dx.doi.org/10.1155/2016/3026745

[41] ASTM – American Society for Testing and Materials. ASTM E606–92: Standard practice for strain controlled fatigue testing. In: Annual Book of ASTM Standards, Part 10; 1998; pp. 557–71. http://dx.doi.org/10.1520/E0606-92R04E01

[42] Ramberg W, Osgood WR. Description of the stress-strain curves by the three parameters. NACA TN-902, National Advisory Committee for Aeronautics, Washington, 1943; 29. http://www.apesolutions.com/spd/public/NACA-TN902.pdf

[43] ASTM—American Society for Testing and Materials. ASTM E647: standard test method for measurement of fatigue crack growth rates. In: Annual book of ASTM Standards, vol. 03.01. West Conshohocken, PA: ASTM—American Society for Testing and Materials; 2000; pp. 591–630.

IntechOpen